Fin sweep angle does not determine flapping propulsive performance

Andhini N. Zurman-Nasution[1,✉], **Bharathram Ganapathisubramani**[1,✉], **and Gabriel D. Weymouth**[1,✉]

[1]Engineering, University of Southampton, Southampton Boldrewood Innovation Campus, UK

The importance of the leading-edge sweep angle of propulsive surfaces used by unsteady swimming and flying animals has been an issue of debate for many years, spurring studies in biology, engineering, and robotics with mixed conclusions. In this work we provide results from an extensive set of three-dimensional simulations of finite foils undergoing tail-like (pitch-heave) and flipper-like (twist-roll) kinematics for a range of sweep angles while carefully controlling all other parameters. No significant change in force and power is observed for tail-like motions as the sweep angle increases, with a corresponding efficiency drop of only $\approx 2\%$. Similar findings are seen in flipper-like motion and the overall correlation coefficient between sweep angle and propulsive performance is 0.1-6.7%. This leads to a conclusion that fish tails or mammal flukes can have a large range of potential sweep angles without significant negative propulsive impact. A similar conclusion applies to flippers; although there is a slight benefit to avoid large sweep angles for flippers, this could be easily compensated by adjusting other hydrodynamics parameters such as flapping frequency, amplitude and maximum angle of attack to gain higher thrust and efficiency.

Biolocomotion | **Flapping foils** | **Bio-mechanical evolution**
Correspondence: ***G.D.Weymouth@soton.ac.uk***

Introduction

A large fraction of swimming and flying animals use propulsive flapping to move, and there are significant potential applications for this biologically inspired form of propulsion in engineering and robotics. As such, significant research effort has been devoted towards understanding and optimizing both the kinematics and morphology of the propulsion surface itself, with a particular emphasis on explaining propulsive efficiency.

The leading edge sweep back angle is a key geometric feature observed in fish tails, mammal flukes, aquatic-animal flippers, and bird and insect wings. There have been extensive studies collecting sweep back angle data from a variety of animal propulsion surfaces. The data in Fig. 1 are collected from marine mammals (1), fish caudal fins (2), flyer wings (3–7), and aquatic animal flippers and pectoral fins (8–15). There is a strong correlation between fin aspect ratio, $\mathcal{AR}$, and kinematics. Undulatory motion (such as pectoral fins of skates and rays) are limited to the low $\mathcal{AR} \approx 2$ fins, while the highest $\mathcal{AR} \geq 8$ region is populated only by flippers and wings which performing rolling and twisting motions, such as penguins and most plesiosaurs. Most fish caudal fins, mammal flukes and many flippers and wing are found in the intermediate $\mathcal{AR}$ region. In contrast, the sweep angle Λ dependence

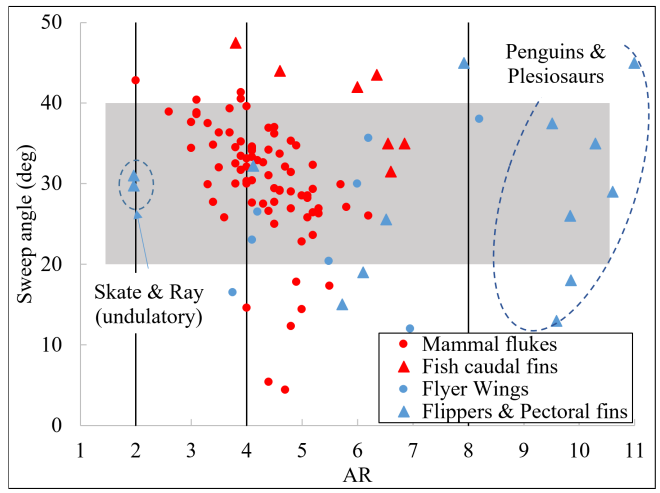

Fig. 1. Collection of biologist data for sweep angles and aspect ratio $\mathcal{AR}$ for fish caudal fins and mammal flukes (in red) and flippers, pectoral fins, and wings (in blue) shows the extremely wide scatter across this evolutionary parameter space for different successful animals. The current computational study takes place over sweep angles from $20 - 40\,\mathrm{deg}$ (grey rectangle) and $\mathcal{AR} = 2, 4, 8$ to maximize the relevance to biological propulsive surfaces.

is much less clear, with flipper and propulsive pectoral fins spanning a wide range of angles. While some individual studies indicate that increased sweep angles are correlated with animals with lower aspect ratios $\mathcal{AR}$ fins, there is extensive variation between animals within the groups and no strong trend is found when including all the groups using propulsive flapping. Additionally, there are hundreds of differences in the specific geometry and kinematics of each of these animals and just as many biological pressures other than propulsive efficiency at play, making it difficult to conclusively determine the influence of sweep angle from biological data directly.

Focused engineering studies have also been applied to determine the impact of sweep angle on the performance of flapping propulsion surfaces. While these would hopefully clarify the issues at play, the finding are somewhat contradictory, especially between theoretical and experimental analysis. Most analytical studies using lifting-line theory indicate sweep is advantageous, increasing the thrust and propulsive efficiency (16–18). While such methodologies are effective at determining lift characteristics on steady wings, they cannot model unsteady rotational three-dimensional flow, including the evolution of vortices that form at the fin's leading edge and tip which lead to the high forces observed in flapping foil propulsion (19, 20).

While some experimental studies have measured a small flap-

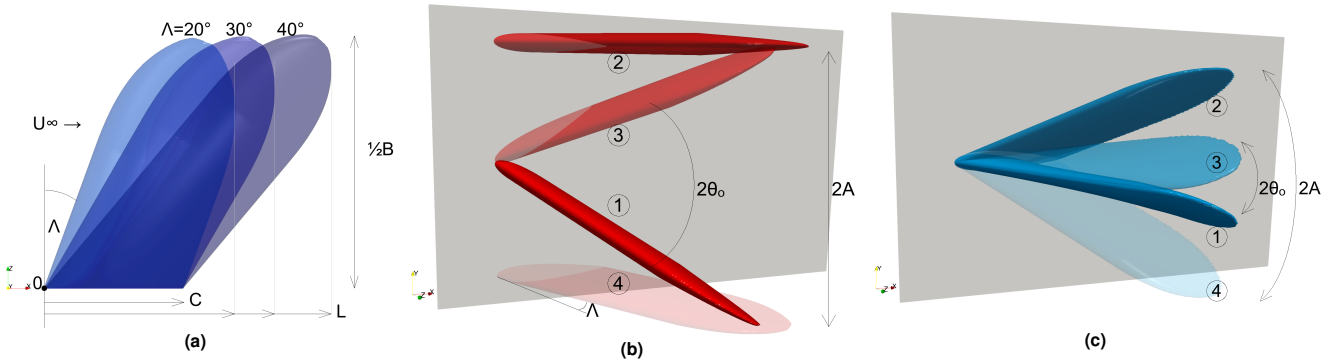

Fig. 2. Diagram of the propulsive fin geometry and kinematics. (a) Foil planform with various sweep angle Λ for two different kinematic i.e. (b) fishtail-like kinematics i.e. pitch-heave combined with $\mathcal{AR} = 4$, and (c) flipper-like kinematics i.e. twist-roll combined with $\mathcal{AR} = 8$. Phase steps per cycle are denoted from ① to ④.

ping propulsive benefit to sweep, the effect is smaller than the analytic studies and other experiments have found no impact at all. A study on the spanwise flow caused by sweep angle found that it did not stabilizing the LEV on an impulsively heaved foil (21), in contrast to the known stabilizing effect on a stationary wing. Another study reported affected forces and vortex strength on a $45°$-sweptback flapping plate for large-scale LEVs produced by an impulsively heaved plate (22). Insignificant force change is also seen in the experiment of manta robot with rolling flexible flippers (23). Varying sweep angle from zero to $60°$ in rotating wings found no influence on the stability of the LEV (24). For a purely pitching flat plate, the data of circulation time-histories show varying reduced frequencies can change the LEV circulation slightly more on the lower frequency cases (25). This indicates that it is important to test a variety of kinematics relevant to the problem, as well as controlling for as many other parameters as possible, something which is very difficult to accomplish in physical experiments.

In this work, we carefully isolate the effect of varied sweep angles from all other geometric parameters to help address the conflicting and scattered results of previous biological, theoretical and experimental studies. Using 3D unsteady numerical simulations, we add sweep to a simple base fin shape and test its flapping propulsive performance for two types of biologically inspired kinematics, i.e. tail-like and flipper-like motions, Fig. 2(a). We also test the combined impact of $\mathcal{AR}$ and sweep as well as other kinematic parameter to determine the relative influence of sweep angle on propulsive flapping.

Specifically, we define our geometry to use a NACA0016 foil cross-section with chord length C, defined parallel to the inflow the U_∞, and thickness $D = 0.16C$. A rectangular planform is combined with a tapered elliptic tip with a length of $1C$. The sweep angle Λ, defined in Fig. 2, is varied from $\Lambda = [20°, 30°, 40°]$ to cover the most populated biological range, Fig. 1. As the sweep is adjusted, the tip-to-tip foil span B is adjusted to maintain the desired aspect ratio $\mathcal{AR} = B^2/S_p$, where S_p is the planform area. As with sweep, we use a wide range of $\mathcal{AR}$ =$[2, 4, 8]$ to cover most propulsive surfaces found in nature. The chord-wise Reynolds number $Re = \rho U_\infty C/\mu = 5300$, where ρ, μ are the fluid density and viscosity, is kept fixed to isolate influence of the geometry and kinematics.

This geometry is subjected to sinusoidal "tail-like" and "flipper-like" motions diagrammed in Fig. 2. The tail-like kinematics are inspired by measurements of fish caudal fins and mammal flukes and made up coupled heave and pitch motions, Fig 2(b). The flipper-like kinematics are inspired by aquatic animal pectoral flippers and bird/insect wings, and is made up twist and roll motions, Fig 2(c). The motion amplitude and frequency are quantified by Strouhal number $St = 2Af/U_\infty$ and reduced frequency $k^* = fl^*/U_\infty$, where f is the motion frequency, $2A$ is the total perpendicular amplitude envelop for the motion, and l^* is a length-scale equal to the total inline extent L for tail-like motions and $B/2$ for flipper-like motions. The majority of the simulations use a fairly low frequency $k^* = 0.3$ and high amplitude $2A = l^*$ condition to imitate the average mammal-fluke kinematics as reported in biological data (1), and the Strouhal number $St = 0.3$ is fixed in the middle of the optimal thrust production range (26). A few special cases outside these conditions were also simulated: A flipper-like motion using higher $k^* = 0.6$ and $St = 0.6$ to imitate penguin and turtle swimming data with high roll and twist angles to maintain high propulsion and efficiency due to high $\mathcal{AR}$. Also, a tail-like motion at lower amplitude $A = 0.13l^*$ and much higher frequency at $St = 0.46$ inspired by recent robotics studies at similar operating conditions (27, 28).

Impact of sweep on wake structures and propulsive characteristics

A set of example simulation results for both tail-like and flipper-like motions are shown in Fig. 3, with the flow's vortex structures visualized using the Q-criterion (28). The complete unsteady flow field evolution can be viewed in the supplementary video. These wake visualizations show that small scale features such as the generation of small turbulent vortices depends on both the geometry and the kinematics. However, the large-scale underlying flow structures illustrated in the bottom row sketches are the same for a given set of kinematics; changing the sweep angle from $20°$ to $40°$ simply shifts and scales those structures. Specifically, for the tail-like motions in the left column, the leading edge vortex detaches from the top of the fin halfway along the inline length $l^* = L$ for tail-like motions. Similarly, while increasing the sweep angle pushes the LEV back for flipper like motions, the separation for both cases occurs around 70% along the fin width

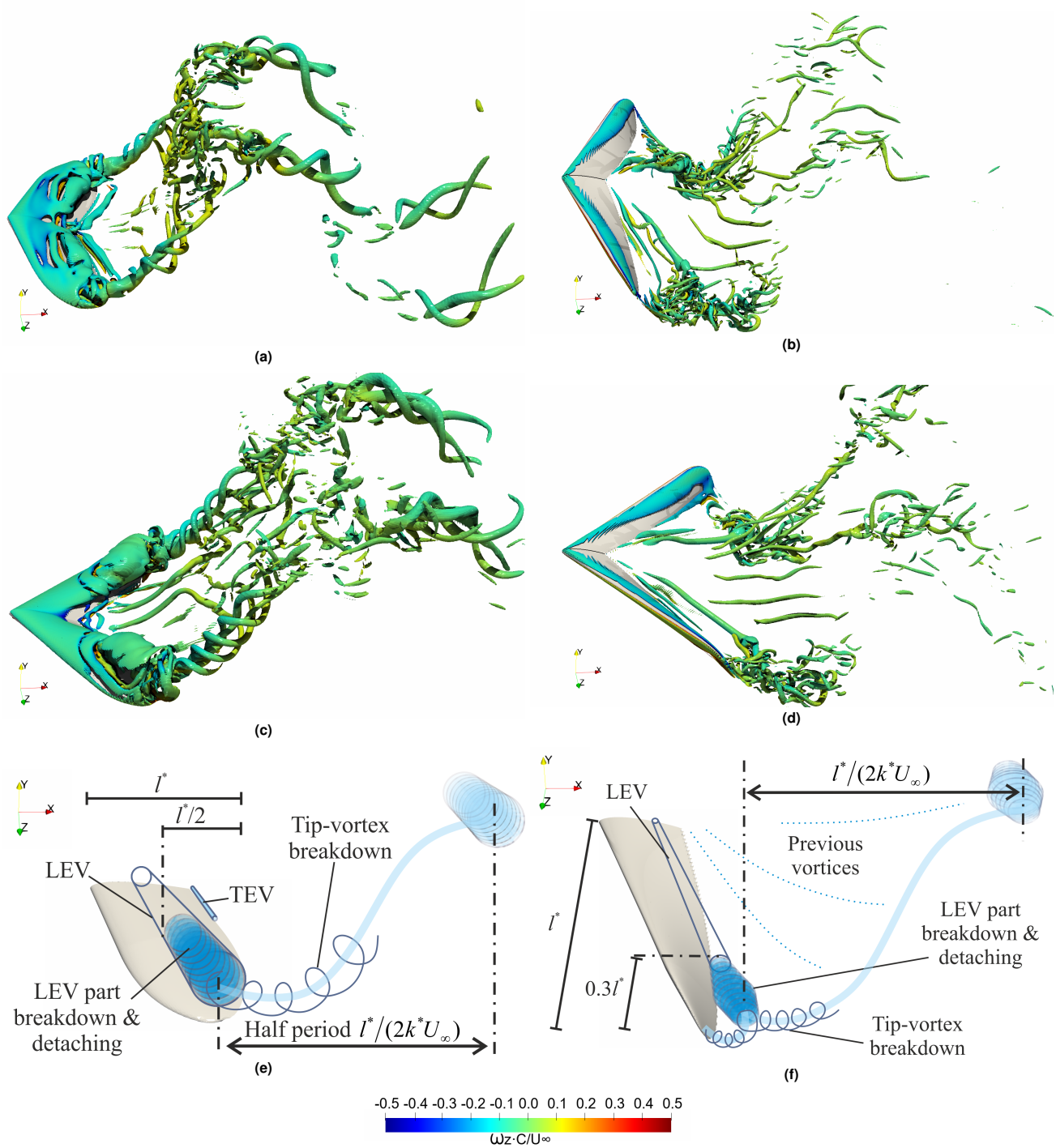

Fig. 3. Flow structures generated by tail-like and flipper-like propulsive swimming at position 1 shown in Fig.2. Tail-like motions are depicted in pitch-heave for (a) $\Lambda 20$, (c) $\Lambda 40$ for $\mathcal{AR}= 4$, and flipper-like motions as in twist-roll for (b) $\Lambda 20$, (d) $\Lambda 40$ for $\mathcal{AR}= 8$. Instantaneous vortex structures are visualized using iso-surfaces with 1% of Q_{max} colored by the spanwise vorticity $\omega_z C/U_\infty$. Illustration of vortex-shedding process every half period ($l^*/(2k^*U_\infty)$) of cycle for (e) tail-like motion and (f) flipper-like.

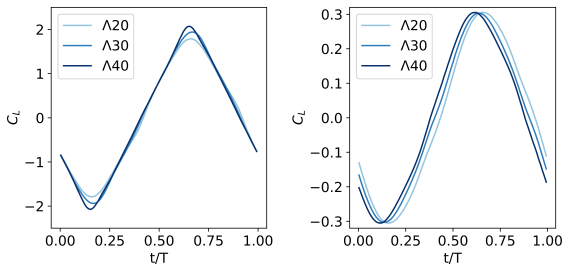

Fig. 4. Lift coefficient of (a) tail-like and (b) flipper-like motion for $\mathcal{AR} = 4$, $St = 0.3$ and $k^* = 0.3$ in one cycle period (T). Both graphs show no LEV detachment delay as Λ increases.

$l^* = B/2$ for these cases. The period and wavelength of the trailing wake structures also scale with l^* because we have used l^* to define the reduced frequency $k*$ and the amplitude envelop $2A = l^*$. In other words, the sweep angle does not fundamentally change the resulting propulsive flow around the fins other than changing the characteristic length l^*.

We can quantify this invariance of the flow in terms of the integrated propulsive metrics; the coefficients of thrust C_T lift C_L and power C_{Pow}, and the propulsive efficiency η, defined as

$$C_T = \frac{F_x}{0.5\rho S_p U_\infty^2}, \qquad C_L = \frac{F_y}{0.5\rho S_p U_\infty^2}, \tag{1}$$

$$C_{Pow} = \frac{P}{0.5\rho S_p U_\infty^3}, \qquad \eta = \frac{\overline{F_x} U_\infty}{\overline{P}} = \frac{\overline{C_T}}{\overline{C_{Pow}}} \tag{2}$$

where measured thrust force (F_x), lift force (F_y), and power (P) are calculated from the integration of pressure and viscous forces over the foil. S_p is the foil planform area and overline signifies cycle averaging.

A sample of the lift coefficient results are shown in Fig.4 for both tail-like and flipper like kinematics across the range of sweep angles. The qualitative and quantitative features of the lift force over the cycle are relatively unaffected by doubling the sweep angle. In particular, our simulation results do not indicate a significant time delay in the peak lift with sweep, meaning that sweep is not changing the stability of the propulsive LEV. This conclusion is supported by the similarity in the LEV appearance on $\Lambda 20°$ and $\Lambda 40°$ in Fig. 3. The thrust coefficient and power also show a similar lack of influence of sweep on hydrodynamic performance. This information is presented in the supplementary material where we present the variation of mean thrust (and its variance) as well as power coefficient (and its variance) and pitching moment for different $\mathcal{AR}$ and kinematics. Overall, our simulations suggest that sweep causes slight variations in the breakdown of the main vortex structures, but this is not observed to have significant impact on the force statistics as well as efficiency. Fig. 5(a) summarises the influence of different input parameters on the hydrodynamic performance using parallel coordinates to simultaneously present the geometric and kinematics inputs and the propulsive statistics outputs. Fig. 5(b) show the correlations between the different inputs and outputs. Here, the main inputs are the motion types, sweep angles, $\mathcal{AR}$s, and flapping amplitude A/l^*. Different St and

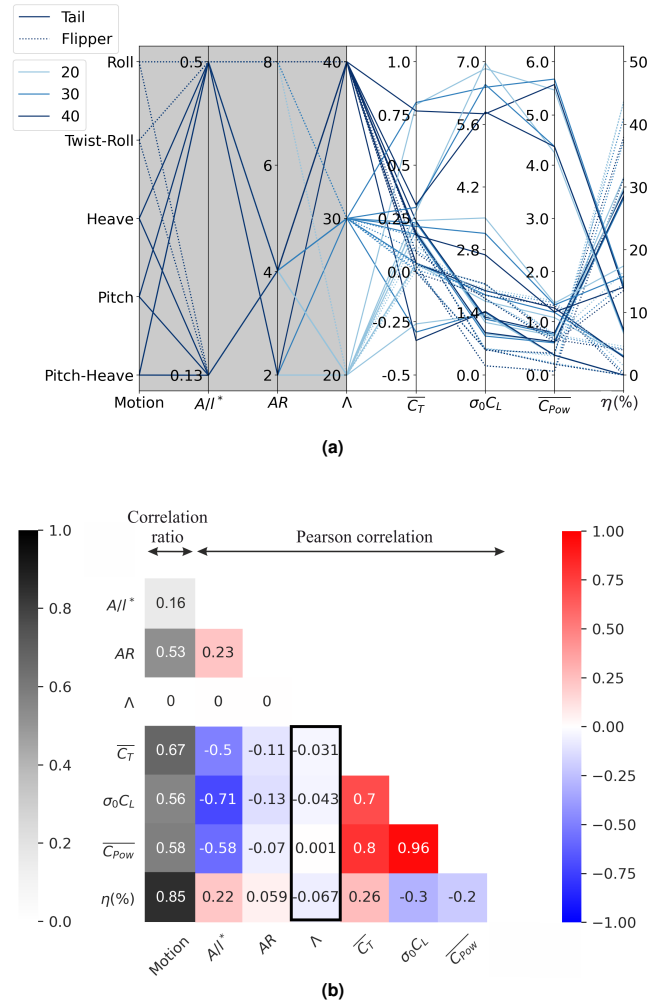

Fig. 5. The relations from 39 simulations among the various inputs and output parameters i.e. the mean thrust coefficient $\overline{C_T}$, amplitude of the lift coefficient measured by the standard deviation $\sigma_0 C_L$, mean power coefficients $\overline{C_{Pow}}$ and efficiency η, are presented in (a) a parallel-coordinate graph with grey shaded inputs, and (b) a heat-map graph of correlation coefficients using Pearson and correlation ratio with a box highlighting Λ correlation. Continuous lines in Fig.(a) are for the tail-like and dotted lines for the flipper-like motions. The lines on the output area of Fig.(a) regroup to their 3-color Λ showing that sweep angles have an insignificant impact on the output in spite of the large input variation convinced by the correlation values in the box of Fig (b).

k^* are represented by two flapping amplitudes for biological-inspired (high amplitude, low frequency) and engineering-inspired (low amplitude, high frequency) motions, whereas different motion types represent the change in α_{max}.

Figure 5 clearly illustrates our primary finding that sweep angle is not responsible for the large potential variation in propulsive statistics. Indeed, the Pearson's correlation between the sweep angle and the propulsive statistics is between 0.1% and 6.7%, whereas the amplitude and motion type (pure roll vs twist-roll etc) are correlated with the force and power coefficients above 50%. The $\mathcal{AR}$ of the propulsive surface is also found to be secondary compared to the kinematics, with the largest (13%) correlation with the standard deviation of the lift coefficient.

Kinematics made up of a combination of degrees of freedom (twist+roll, heave+pitch) are seen to be more beneficial than single degree of freedom (DOF) motions (pure pitch, heave, or roll) as shown in Fig 5(a). The efficiencies above 25%

belong to the cases with combined motions and higher amplitude (biological-inspired) conditions, with flipper-like motion giving the highest efficiency. All types of motion with lower amplitude (engineering-inspired) give efficiencies between 4%-20% with combined DOF motions and pure pitching giving efficiencies above 10%. Single DOF motions in animal operating condition gives no benefit at all. In addition, the penguin-like flipper case has a high ≈40% efficiency which is achievable because the long span and large twist amplitude combine to achieve a similar maximum angle of attack along the span (29). Finally, we note that the tail-like motions produce relatively higher $\overline{C_T}$ than the flipper-like motions. Overall it is clear that kinematic parameters are more influential than the planform geometry for propulsive optimization.

Conclusion

In conclusion, we have studied the influence of fin sweep angle and $\mathcal{AR}$ on flapping foil propulsive performance using a set of high resolution three dimensional viscous flow simulations. This enables us to more tightly control all other geometric and kinematic parameters than would be possible in biological or experimental studies, producing an extensive and focused data set of flow fields, integrated forces, and propulsive efficiencies. Generally, we have seen no advantages for having sweptback leading-edge of flapping with tail-like motions. Perhaps more importantly, having swept planform also does not lead to a significant disadvantage. This can explain why biological data for sweep angle of fish caudal fins and mammal flukes have a large observed range and are not strongly correlated with kinematics or fin aspect ratio. From a biological perspective, this signifies that the so-called fastest fishes from Scombridae family or mammals from Delphinidae family can have either high or low sweep angle given any $\mathcal{AR}$ range without losing thrust and affecting their propulsive efficiency. Similarly, increased sweep angle does not give an advantage to flipper-like motions, instead tending to lose efficiency due to increased power requirements and loss of thrust. However, this loss is small, typically less than 10%, and can be compensated by increasing tip frequency, Strouhal number, and twist angle to recover the lost thrust force. The sweep angle also does not affect the lift coefficient, which is beneficial as flippers are also used as a lift regulator in animal swimming (30).

This study finds no benefit to sweep for steady-speed swimming, but does this does not preclude other more subtle potential fluid dynamic advantages. For example, in very high velocity motions more similar to animal maneuvering than steady swimming (31), experiments have observed a modulated C_L peak for $\Lambda 45°$ compared to $\Lambda 0°$ (22). In addition, previous simulations have show that fin-to-fin interactions may have an important effect on increasing propulsive efficiency (32). As such, is it still possible that sweptback angle may impart an advantage, despite not making a significant contribution to steady swimming efficiency. This finding should help focus research in these more fruitful directions, and simplify the design of potential biologically-inspired vehicles and robots.

Methods

The prescribed form of the heaving $\mathcal{H}(t)$ and pitching $\theta(t)$ functions are given by

$$\mathcal{H}(t) = A\sin(2\pi f t) \tag{3}$$

$$\theta(t) = \theta_0 \sin(2\pi f t + \psi) \tag{4}$$

$$\theta_0 = \sin^{-1}(A/l^*) \tag{5}$$

where θ_0 the trailing-edge tip rotation amplitude, and the phase difference $\psi = 90°$ are set based on the maximum performance for 2D motions (33). The twist is defined equivalently to pitch, with the amplitude increasing with distance from the root section. The pivot point of pitch and twist is at the leading edge of the root section. The roll motion is simply rotation about the inline axis, and the amplitude is set to achieve the same amplitude A.

The correlation methods in Fig. 5 (b) use widely known Pearson coefficient of correlation between two continuous sets of data, and correlation ratio between a category set and a continuous data set. A correlation ratio is defined as

$$\sqrt{\frac{\sum_x n_x(\overline{y}_x - \overline{y})^2}{\sum_{x,i}(y_{xi} - \overline{y})^2}} \tag{6}$$

where

$$\overline{y}_x = \frac{\sum_i y_{x,i}}{n_x}, \quad \overline{y} = \frac{\sum_x n_x \overline{y}_x}{\sum_x n_x}, \tag{7}$$

x category in each observation y_{xi}, i index, n_x the number of observation in category x, and $\overline{y}_x$ is the mean of category x.

The computational package used for this research is the Boundary Data Immersion Method (BDIM) (34). BDIM uses a robust and efficient Cartesian grid with an implicit LES (iLES) solver. BDIM uses analytic meta-equations for an immersed body in multi-phase flow with a smoothed interface domain using an integral kernel. BDIM has been validated, proved suitable for moving bodies and capable of resolving the flow at $Re = 10^5$ within 5% error for thrust prediction (35).

Symmetric conditions are enforced on both spanwise boundaries for the finite foil simulation. The domains extend from the pivot point to $4C$ at the front, $11C$ at the rear, $5.5C$ at the top and bottom. Meanwhile, the tip distance to the maximum spanwise domain is $3.2C$. The grid convergence study provided in (20) using an infinite foil with a span length of $6C$ in $Re = 5300$ as a comparison of time-averaged thrust coefficient for different resolutions. The force coefficient converges to within 7% of the finer simulations (for 2D and 3D simulation) using a resolution of $C/\Delta x = 128$. As a balance between the grid resolution and the number of simulations, this resolution is deemed sufficient to captures the dynamics of the flow.

ACKNOWLEDGEMENTS
We would like to thank Indonesia Endowment Fund for Education (LPDP), IRIDIS High Performance Computing Facility with its associated support services at the University of Southampton and the Office of Naval Research Global award N62909-18-1-2091 for the completion of this work. We also want to thank Professor George V. Lauder (Harvard) for constructive discussions.

Bibliography

1. F. E. Fish and Rohr. J. J. Review of dolphin hydrodynamics and swimming performance. Technical report, SSC San Diego, 1999.
2. J. J. Magnuson. Locomotion by scombrid fishes: Hydromechanics, morphology, and behavior. In W.S. Hoar Randall and D.J., editors, *Locomotion*, volume 7, pages 239–313. Academic Press, 1978.
3. T. Y. Hubel, N. I. Hristov, S. M. Swartz, and K. S. Breuer. Wake structure and kinematics in two insectivorous bats. *Philos Trans R Soc Lond B Biol Sci*, 371(1704):1–12, 2016. doi: 10.1098/rstb.2015.0385.
4. R. Von Busse, A. Hedenstrom, Y. Winter, and L. C. Johansson. Kinematics and wing shape across flight speed in the bat, leptonycteris yerbabuenae. *Biol Open*, 1(12):1226–38, 2012. doi: 10.1242/bio.20122964.
5. B. Klaassen van Oorschot, E. A. Mistick, and B. W. Tobalske. Aerodynamic consequences of wing morphing during emulated take-off and gliding in birds. *J Exp Biol*, 219(Pt 19): 3146–3154, 2016. doi: 10.1242/jeb.136721.
6. A. P. Willmott and C. P. Ellington. The mechanics of flight in the hawkmoth manduca sexta. ii. aerodynamic consequences of kinematic and morphological variation. *J Exp Biol*, 200(Pt 21):2723–45, 1997.
7. C. J. Pennycuick. A wind-tunnel study of gliding flight in the pigeon columba livia. *J Exp Biol*, 49(3):509–526, 1968.
8. R. Gurdek Bas, W. Serra, R. Trinchin, V. Leoni, L. Rubio, L. Sampognaro, G. Nagy, A. Cravino, and A. Acuña. Confirmation of mola mola (tetraodontiformes: Molidae) and historical records of ocean sunfishes (mola sp.) in the coastal area of uruguay. *Marine Biodiversity Records*, 8:1–5, 2015. doi: 10.1017/s1755267214001468.
9. F. E. Fish and J. M. Battle. Hydrodynamic design of the humpback whale flipper. *J Morphol*, 225(1):51–60, 1995. doi: 10.1002/jmor.1052250105.
10. K. Carpenter, F. Sanders, B. Reed, J. Reed, and P. Larson. Plesiosaur swimming as interpreted from skeletal analysis and experimental results. *Transactions of the Kansas Academy of Science*, 113(1/2):1–34, 2010. doi: 10.2307/40588253.
11. A. R. Rivera, G. Rivera, and R. W. Blob. Forelimb kinematics during swimming in the pig-nosed turtle, carettochelys insculpta, compared with other turtle taxa: rowing versus flapping, convergence versus intermediacy. *J Exp Biol*, 216(Pt 4):668–80, 2013. doi: 10.1242/jeb.079715.
12. K. Sato, K. Shiomi, Y. Watanabe, Y. Watanuki, A. Takahashi, and P. J. Ponganis. Scaling of swim speed and stroke frequency in geometrically similar penguins: they swim optimally to minimize cost of transport. *Proc Biol Sci*, 277(1682):707–14, 2010. doi: 10.1098/rspb.2009.1515.
13. R. S. Russo, S. S. Blemker, F. E. Fish, and H. Bart-Smith. Biomechanical model of batoid (skates and rays) pectoral fins predicts the influence of skeletal structure on fin kinematics: implications for bio-inspired design. *Bioinspir Biomim*, 10(4):046002, 2015. doi: 10.1088/1748-3190/10/4/046002.
14. J. M. D. Astarloa, E. Mabragana, and R. Hanner. Morphological and molecular evidence for a new species of longnose skate (rajiformes: Rajidae: Dipturus) from argentinean waters based on dna barcoding. *Zootaxa*, 1921:35–46, 2008. doi: 10.5281/zenodo.184713.
15. J. M. Rambahiniarison, G. Araujo, M. J. Lamoste, J. Labaja, S. Snow, and A. Ponzo. First records of the reef manta ray manta alfredi in the bohol sea, philippines, and its implication for conservation. *Journal of Asia-Pacific Biodiversity*, 9(4):489–493, 2016. doi: 10.1016/j.japb.2016.07.002.
16. P. Liu and N. Bose. Propulsive performance of three naturally occurring oscillating propeller planforms. *Ocean Engineering*, 20(1):57–75, 1993. doi: 10.1016/0029-8018(93)90046-k.
17. C. P. van Dam. Efficiency characteristics of crescent-shaped wings and caudal fins. *Nature*, 325(6103):435–437, 1987. doi: 10.1038/325435a0.
18. M. G. Chopra and T. Kambe. Hydromechanics of lunate-tail swimming propulsion. part 2. *Journal of Fluid Mechanics*, 79(1):49–69, 2006. doi: 10.1017/s0022112077000032.
19. T. S. Liu, S. Z. Wang, X. Zhang, and G. W. He. Unsteady thin-airfoil theory revisited: Application of a simple lift formula. *Aiaa Journal*, 53(6):1492–1502, 2015. doi: 10.2514/1.J053439.
20. A. N. Zurman-Nasution, B. Ganapathisubramani, and G. D. Weymouth. Influence of three-dimensionality on propulsive flapping. *Journal of Fluid Mechanics*, 886:1–14, 2020. doi: 10.1017/jfm.2019.1078.
21. H. R. Beem, D. E. Rival, and M. S. Triantafyllou. On the stabilization of leading-edge vortices with spanwise flow. *Experiments in Fluids*, 52(2):511–517, 2011. doi: 10.1007/s00348-011-1241-9.
22. J. G. Wong, J. Kriegseis, and D. E. Rival. An investigation into vortex growth and stabilization for two-dimensional plunging and flapping plates with varying sweep. *Journal of Fluids and Structures*, 43:231–243, 2013. doi: 10.1016/j.jfluidstructs.2013.09.010.
23. S. Arastehfar, C. M. Chew, A. Jalalian, G. Gunawan, and K. S. Yeo. A relationship between sweep angle of flapping pectoral fins and thrust generation. *Journal of Mechanisms and Robotics-Transactions of the Asme*, 11(1):1–17, 2019. doi: Artn01101410.1115/1.4041697.
24. D. Lentink and M. H. Dickinson. Rotational accelerations stabilize leading edge vortices on revolving fly wings. *J Exp Biol*, 212(Pt 16):2705–19, 2009. doi: 10.1242/jeb.022269.
25. K. Onoue and K. S. Breuer. A scaling for vortex formation on swept and unswept pitching wings. *Journal of Fluid Mechanics*, 832:697–720, 2017. doi: 10.1017/jfm.2017.710.
26. M. S. Triantafyllou, G. S. Triantafyllou, and R. Gopalkrishnan. Wake mechanics for thrust generation in oscillating foils. *Physics of Fluids a-Fluid Dynamics*, 3(12):2835–2837, 1991. doi: Doi10.1063/1.858173.
27. J. Zhu, C. White, D. K. Wainwright, V. Di Santo, G. V. Lauder, and H. Bart-Smith. Tuna robotics: A high-frequency experimental platform exploring the performance space of swimming fishes. *Science Robotics*, 4(34):1–12, 2019. doi: ARTNeaax461510.1126/scirobotics.aax4615.
28. J. T. King, R. Kumar, and M. A. Green. Experimental observations of the three-dimensional wake structures and dynamics generated by a rigid, bioinspired pitching panel. *Physical Review Fluids*, 3(3):1–20, 2018. doi: ARTN03470110.1103/PhysRevFluids.3.034701.
29. A. N. Zurman-Nasution, B. Ganapathisubramani, and G. B. Weymouth. Effects of aspect ratio on rolling and twisting foils, 2020.
30. L. N. Cooper, N. Sedano, S. Johansson, B. May, J. D. Brown, C. M. Holliday, B. W. Kot, and F. E. Fish. Hydrodynamic performance of the minke whale (balaenoptera acutorostrata) flipper. *J Exp Biol*, 211(Pt 12):1859–67, 2008. doi: 10.1242/jeb.014134.
31. D. A. Read, F. S. Hover, and M. S. Triantafyllou. Forces on oscillating foils for propulsion and maneuvering. *Journal of Fluids and Structures*, 17(1):163–183, 2003. doi: PiiS0889-9746(02)00115-9Doi10.1016/S0889-9746(02)00115-9.
32. P. Han, G. V. Lauder, and H. Dong. Hydrodynamics of median-fin interactions in fish-like locomotion: Effects of fin shape and movement. *Physics of Fluids*, 32(1):1–14, 2020. doi: 10.1063/1.5129274.
33. K. Isogai, Y. Shinmoto, and Y. Watanabe. Effects of dynamic stall on propulsive efficiency and thrust of flapping airfoil. *Aiaa Journal*, 37(10):1145–1151, 1999. doi: Doi10.2514/2.589.
34. G. D. Weymouth and D. K. P. Yue. Boundary data immersion method for cartesian-grid simulations of fluid-body interaction problems. *Journal of Computational Physics*, 230(16): 6233–6247, 2011. doi: 10.1016/j.jcp.2011.04.022.
35. A. P. Maertens and G. D. Weymouth. Accurate cartesian-grid simulations of near-body flows at intermediate reynolds numbers. *Computer Methods in Applied Mechanics and Engineering*, 283:106 – 129, 2015. doi: https://doi.org/10.1016/j.cma.2014.09.007.